Astron. Astrophys. 281, 269–280 (1994)

ASTRONOMY AND ASTROPHYSICS

Pole, albedo and shape of the minor planets 624 Hektor and 43 Ariadne: two tests for comparing four different pole determination methods*

A. Detal[1], O. Hainaut[1,2], A. Pospieszalska-Surdej[1], P. Schils[1], H.J. Schober[3], and J. Surdej[1] **

[1] Institut d'Astrophysique, Université de Liège, 5 Avenue de Cointe, B-4000 Liège, Belgium
[2] European Southern Observatory, Karl-Schwarzschild-Straße, 2, D-85748 Garching-bei-München, Germany
[3] Institut für Astronomie, Universitätsplatz, A-8010 Graz, Austria

Received November 25, 1992; accepted July 22, 1993

Abstract. Asteroids 624 Hektor and 43 Ariadne have been observed photometrically at the European Southern Observatory (La Silla, Chile) in order to determine their pole orientation. The lightcurves (1984 and 1991 oppositions for Hektor, and 1985 for Ariadne) are presented. Some of the traditional pole determination methods have been improved, and completely original ones have been developed. They are described and applied to the newly recorded and previously published lightcurves. The results are commented and compared with previous ones. In addition to the pole orientation, we also derive some information on the shape or the albedo distribution of the objects. With the aim of optimizing future observations of these asteroids, we present some graphs showing the best longitudes where they should be measured. Finally, we suggest some improvements in the pole determination and modeling methods based upon photometric data.

Key words: asteroids – pole orientation – asteroids: shape – asteroids: albedo – 624 Hektor – 43 Ariadne

1. Introduction

Minor planets have been subject to various kinds of interaction during their evolution: mutual collisions, gravitational perturbations by Jupiter, etc... An accurate determination of the distribution of their rotation axes should contribute to a better understanding of the history of our Solar System. Several methods have been developed to find the pole orientation of an asteroid. Among them, those using photometric lightcurves are not the most efficient ones, but they are very convenient to use on a large sample of objects. Indeed, photometric data are easy to collect (a small size telescope is sufficient) and many archive data are available (cf. Lagerkvist et al. 1987 and 1988), covering a long time scale, while most of the other methods need very specialized instruments (large telescope, speckle camera...), and have been applied to very few objects. In this context, we have initiated several years ago a campaign of photometric observations of minor planets at the European Southern Observatory (some results in Pospieszalska-Surdej & Surdej 1985; Surdej et al. 1986; Hainaut & Detal 1992).

New photometric lightcurves have been recorded for 624 Hektor during its 1984 and 1991 oppositions, and for 43 Ariadne during its 1985 opposition. These observations are presented in Appendix.

Several methods to find the pole orientation of an asteroid have been developed. In Sect. 2, we describe in detail four of them, which are either improvements of traditional methods, or completely original ones. The Revisited Amplitude/Magnitude-Aspect method is based on a triaxial ellipsoid model, the Free Albedo Map method on a sphere covered with many surface elements which albedoes are adjusted, and the Free Shape method on a deformable polyhedron. The Photometric Astrometry allows one to retrieve the pole orientation from the small variations in the synodic rotational period measured at various positions of the asteroid.

In Sect. 3, we apply these methods to both the newly obtained and previously published photometric lightcurves of 624 Hektor and 43 Ariadne . These results are then compared between each other and with other authors' pole determinations. Discussion and conclusions form the last section.

Send offprint requests to: A. Detal

* Based on observations collected at the European Southern Observatory, La Silla, Chile

** also Maître de recherches au Fonds National de la Recherche Scientifique (Belgium)

2. Description of the pole determination methods

In this section, all the observed fluxes considered are normalized to $R = \Delta = 1$AU.

2.1. The Revised Amplitude/Magnitude-Aspect method (RAMA)

This method is derived from the magnitude-aspect method (Surdej et al. 1986). Let us assume that the shape of the asteroid is a triaxial ellipsoid (semi-axes $a > b > c$) with a uniform albedo and that the diffusion is geometric (the reflected flux is proportional to the area of the diffusing surface projected on the plane of the sky).

The projected surface of the ellipsoid at given aspect A and rotational phase Ψ angles may be expressed as

$$S(\Psi) = \pi abc \sqrt{\sin^2 A \left(\frac{\sin^2 \Psi}{a^2} + \frac{\cos^2 \Psi}{b^2} \right) + \frac{\cos^2 A}{c^2}} \; . \qquad (1)$$

At a solar phase α, the ellipsoid is not completely illuminated. This affects the expression of the effective diffusing surface in a complicated way, but Pospieszalska-Surdej & Surdej (1985) showed that this shadowing is a second order effect. It can be neglected for the small values of α. The other phase effects are described by the multiple scattering theory for atmosphereless bodies (Lumme & Bowell 1981 a and b). F, the observed flux, may be expressed by the relation

$$F(\Psi, \alpha) = \frac{F(\Psi, \alpha = 0°)}{g(Q, \alpha)} \qquad (2)$$

$$= \frac{F_\odot \; x \; S(\Psi)}{g(Q, \alpha)} \; , \qquad (3)$$

where $F_\odot$ is the illuminating flux, x the geometric albedo and g gives the distribution between the single and multi-scattered light. It is defined by

$$g(Q, \alpha) = (Q + (1 - Q) f(\alpha))^{-1} \; , \qquad (4)$$

where $f(\alpha)$ is the phase function for single scattered light (Lumme & Bowell 1981 a and b), and Q is the multiple scattering parameter.

Using relation (1) for S, Eq. (3) may be rewritten as

$$F^2(\Psi, \alpha) = \frac{F_\odot^2 \; x^2 \pi^2 a^2 b^2 c^2}{g^2(Q, \alpha)}$$
$$\left(\sin^2 A \left(\frac{-1}{a^2} + \frac{1}{b^2} \right) \cos^2 \Psi + \left(\frac{\sin^2 A}{a^2} + \frac{cos^2 A}{c^2} \right) \right) \; . \qquad (5)$$

The lightcurve equation becomes

$$F^2(\Psi, \alpha) = B \cos^2 \Psi + C \; , \qquad (6)$$

where B and C are defined by

$$B = \frac{(F_\odot \; x \pi bc)^2}{g^2(Q, \alpha)} \left(\frac{a^2}{b^2} - 1 \right) (1 - \cos^2 A) \; , \qquad (7)$$

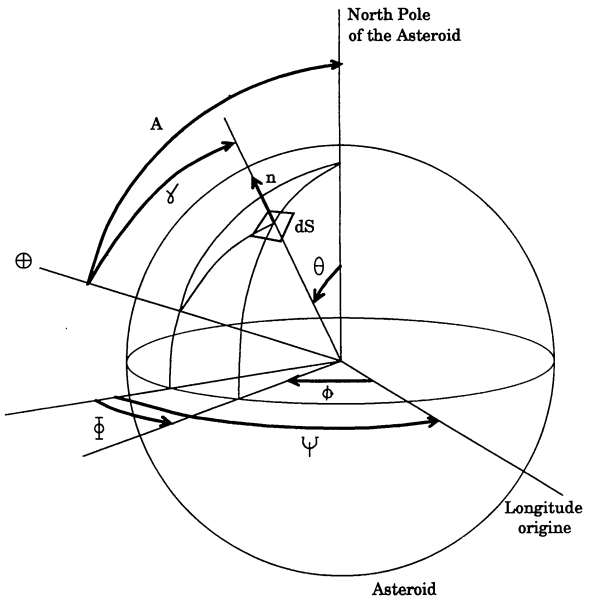

Fig. 1. Geometry of the diffusion by one facet in the FAM model

and

$$C = \frac{(F_\odot \; x \pi bc)^2}{g^2(Q, \alpha)} \left(1 + \cos^2 A \left(\frac{a^2}{c^2} - 1 \right) \right) \; . \qquad (8)$$

Note that F^2 is a linear function of $\cos^2 \Psi$. Replacing the values of $\cos^2 A$ extracted from Eqs. (7) and (8) into its spherical trigonometric expression, one gets the two fundamental equations of the Revisited Amplitude/Magnitude-Aspect relation:

$$(\sin\beta \sin\beta_o + \cos\beta \cos\beta_o \cos(\lambda - \lambda_o))^2$$
$$- \left(1 - \frac{B g^2(Q, \alpha)}{\left(\frac{a^2}{b^2} - 1 \right) (\pi bc)^2} \right) = 0 \; ; \qquad (9)$$

$$(\sin\beta \sin\beta_o + \cos\beta \cos\beta_o \cos(\lambda - \lambda_o))$$
$$- \left(\frac{C g^2(Q, \alpha)}{(\pi bc)^2} - 1 \right) \left(\frac{a^2}{b^2} \frac{b^2}{c^2} - 1 \right)^{-1} = 0 \; . \qquad (10)$$

Using a linear least square fit of the photometric data by means of Eq. (6), each single lightcurve will provide a numerical value for B and C. A system of equations is then built by replacing the B, C, λ and β corresponding to each lightcurve in Eqs. (9) and (10). It can be solved by a minimization technique leading directly to the values of the unknowns λ_o, β_o, a, b, c and Q. We usually prefer to scan the whole celestial sphere (with a typical 1–10° step in both λ_o and β_o), and fit the four remaining parameters for each trial pole orientation. The resulting χ^2 are plotted as a contour map in the (λ_o, β_o) coordinate system. While a simultaneous fit of the six parameters leads very quickly to a solution, the χ^2 map gives a global vision of the whole sky. It does not only show the best pole orientation, but also the secondary solutions and give an estimate of the uncertainty region

for the pole. Examples of these χ^2 maps are presented in the next section for 624 Hektor and 43 Ariadne (cf. Figs. 6 and 7).

The RAMA technique makes full use of the photometric information contained in the lightcurves (amplitude *and* magnitude, through the fit of B and C over all observational points), and not only the amplitude *or* the magnitude of selected extrema, as in the previous methods. Moreover, it is computationally cheap and the longitude of the rotational axis is obtained with a high precision. However, as the shape model is very rough, the information on the asteroid morphology is poor.

2.2. *The Free Albedo Map method (FAM)*

H.N. Russell showed in a very general way that the lightcurves of any convex body, with no restriction about its albedo, can be reproduced by a suitable albedo distribution on a sphere (Russell 1906). The geometry of the spherical model (rotation axis and sidereal period, position...) must be the same as that for the asteroid. We used this "Russell law" to represent the asteroid with a spherical model approximated by a finite set of small surface elements with varying albedoes.

The flux received from one of these small surface elements is

$$\mathrm{d}F = F_\odot \; x \;\; \mathrm{d}S \;\; \cos^+\gamma \; , \tag{11}$$

where $\cos^+$ is equal to the cosine if it is positive (ie for an argument in $[-90^o, +90^o]$), null otherwise. γ is the angle formed by the normal of the element and the line-of-sight (cf. Fig. 1). The $\cos^+$ function discriminates between the visible and hidden elements. Let θ and ϕ be the position angles of the surface element center (cf. Fig. 1). θ is its colatitude, and ϕ the angle between the meridians containing the element center and a fixed meridian of the asteroid. Ψ being the rotational phase (defined as the angle between the fixed reference meridian of the asteroid and the meridian containing the sub-Earth point), the angle Φ between the meridians of the sub-earth point and of the surface element center is related to ϕ by

$$\phi = \Phi - \Psi \; . \tag{12}$$

By means of spherical trigonometry, we may write

$$\cos\gamma = \cos A \cos\theta + \sin A \sin\theta \cos(\phi + \Psi) \; . \tag{13}$$

The bidimensional integration of dF over the whole sphere then corresponds to the total flux received by the observer. Let R be the radius of the sphere. It is left as a free parameter, acting as a scaling factor. With $\mathrm{d}S = R^2 \;\sin\theta \; \mathrm{d}\theta \; \mathrm{d}\phi$, the expression of F becomes

$$F = \int_{\phi=0}^{2\pi} \int_{\theta=0}^{\pi} F_\odot \; x(\theta,\phi) \;\; \cos^+\gamma \; R^2 \;\; \sin\theta \; d\theta d\phi \; . \tag{14}$$

This expression assumes that all the surface elements visible from the Earth are illuminated. This is true only at opposition but, as in the ellipsoidal case (Sect. 2.1.), this is still valid at small solar phase angles.

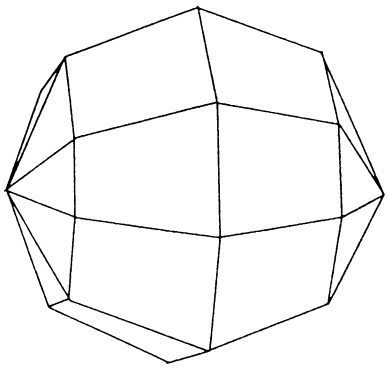

Fig. 2. A polyhedron used with the FAM method; this example corresponds to a rough modeling of the lightcurve (4 × 8 facets)

In practice, for a better computational efficiency, the sphere is approximated by a polyhedron, which facet albedoes are adjusted to reproduce the lightcurves. The surface element boundaries are the equidistant meridians and parallels defined by the number of facets (cf. Fig. 2). The only limitation to this number is the computing time. Typically, we work with up to 16 elements in latitude and 32 in longitude. The area of one of these facets (identified by i) is

$$\Delta S_i = R^2 \;\; \sin\Theta_i \; \Delta\phi_i \; \Delta\theta_i \; , \tag{15}$$

where Θ_i is the colatitude of the facet center, and $\Delta\theta_i$ and $\Delta\phi_i$ its extension in latitude and longitude. Eq. (14) becomes

$$F = F_\odot \; R^2 \sum_{\theta,\,\phi} x_i \;\; \cos^+\gamma_i \;\; \sin\Theta_i \; \Delta\theta_i \; \Delta\phi_i \; . \tag{16}$$

This flux expression is modified to take into account the solar phase effects. Like in the RAMA method (cf. Eq. (4)), we just divide it by the Bowell & Lumme function $g(Q,\alpha)$. So, the flux is now

$$F = \frac{F_\odot \; R^2}{g(Q,\alpha)} \sum_{\theta,\,\phi} x_i \;\; \cos^+\gamma_i \;\; \sin\Theta_i \; \Delta\theta_i \; \Delta\phi_i \; . \tag{17}$$

The observed lightcurves are composed of single points (identified by the subscript k), each corresponding to a geometry defined by the angles Ψ_k and A_k (which is a function of the real pole orientation). Let F_k^{Obs} be that measured flux. For a given trial orientation of the rotational axis of the spherical model ($\lambda_o^{\mathrm{Trial}}$, β_o^{Trial}), the albedoes of the facets x_i as well as the scale factor R and multiple scattering parameter Q are adjusted so that the model's lightcurves fit at best the observed ones. Some of the published lightcurves only give the variations of magnitude (no zero points); in that case, the observed and modeled magnitudes are normalized to the mean of the considered lightcurve. Finally, the minimized quantity is

$$K^2(\lambda_o^{\mathrm{Trial}}, \beta_o^{\mathrm{Trial}}) = \sum_{\text{Abs. LC.}} (F_k^{\mathrm{Obs}} - F_k)^2 \; +$$

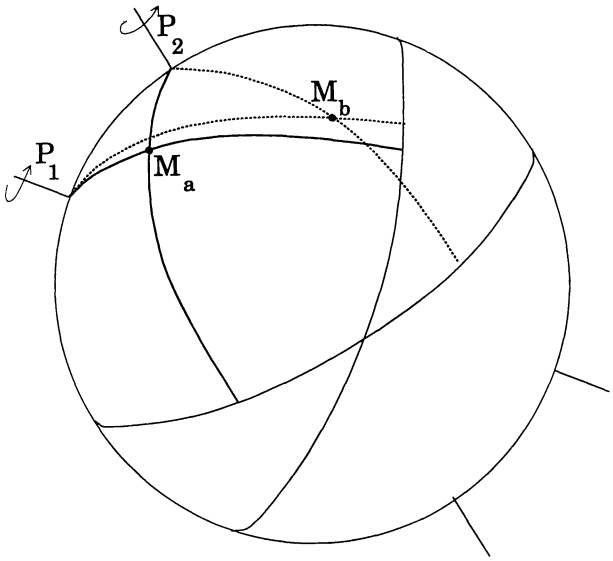

Fig. 3. The origin of the difference between the synodic and sidereal periods of rotation; P_1 and P_2 are two possible poles; M_a and M_b are the PABs corresponding to two different observations

$$\sum_{\text{Rel. LC.}} \left(\frac{F_k^{\text{Obs}}}{\sum_{\text{Considered LC.}} F_k^{\text{Obs}}} - \frac{F_k}{\sum_{\text{Considered LC.}} F_k} \right)^2 ; \qquad (18)$$

where "Abs. LC." and "Rel. LC." refer to the absolute and relative lightcurves that are respectively taken into the sums, and "Considered LC." to the points of the considered lightcurve.

The Russell law being valid only when the pole of the model matches the real pole, $\chi^2(\lambda_o^{\text{Trial}}, \beta_o^{\text{Trial}})$, the minimum value of $K^2(\lambda_o^{\text{Trial}}, \beta_o^{\text{Trial}})$, is a good quality indicator for the trial pole. Like for the RAMA method, the whole celestial sphere is scanned with trial poles $(\lambda_o^{\text{Trial}}, \beta_o^{\text{Trial}})$. For each trial pole, an albedo map, a radius and a multiple scattering parameter are fitted to match at best the observed lightcurves. The χ^2 are then plotted as a contour map in the λ_o, β_o coordinate system, and the best poles are identified. The resulting χ^2 maps for minor planets 624 Hektor and 43 Ariadne are given in the next section.

The coding of this algorithm has been performed in FORTRAN 77. The source was carefully optimized to run on a IBM 3090/VF vectorial mainframe. Typically, a χ^2 map needs around 6 hours of CPU time, mostly (95%) on the vectorial processor. The advantages of FAM over RAMA, making this new method more powerful, is that it takes into account each individual point from the lightcurves and not only global values such as B and C in the RAMA method. The FAM model may also reproduce nearly all kinds of lightcurves, and not only ellipsoidal ones. As the RAMA method, it has a much better accuracy on the longitude than on the latitude.

The albedo map(s) obtained for the best pole(s) have to be considered very suspiciously. Indeed, Russell (1906) showed that adding any combination of odd spherical harmonics to the albedo distribution does not change the resulting lightcurves. The best albedo map is so only one among an infinity of equivalent solutions. Moreover, the real asteroid shape is probably very different from a sphere. The pseudo-albedo of a facet is related to the ratio between the real albedo and the local curvature of the asteroid in that considered region (Russell 1906).

2.3. The Free Shape method (FS)

While the FAM method reproduces the observed lightcurves by adjusting the albedo distribution over a sphere, the "Free Shape" method does it by adapting the model shape, while keeping constant the albedo all over the surface.

The surface of the model is formed by many triangular plane facets (cf. Fig. 4). They are built by joining selected points on three adjacent axes emerging from the geometric center of the asteroid. To modify the shape, one has just to adjust the distances between the center of the asteroid and the facet summits (R_i, which are going to be the free parameters of the model) while keeping the axis orientation fixed.

Let us consider one of these facets. Let i, j and k be its summits. The unit vector normal to the facet is

$$\overline{\mathrm{n}} = \frac{\overline{\mathrm{ki}} \wedge \overline{\mathrm{kj}}}{\| \overline{\mathrm{ki}} \wedge \overline{\mathrm{kj}} \|} \qquad (19)$$

($\wedge$ is the vectorial product). Its orientation is chosen to point outward the polyhedron. The facet area is

$$\Delta S = \frac{1}{2} \| \overline{\mathrm{ki}} \wedge \overline{\mathrm{kj}} \| . \qquad (20)$$

Close to the opposition, the flux reflected by the facet is

$$\Delta F = \frac{F_\odot \, x}{g(Q, \alpha)} \cos^+ \gamma \, \Delta S , \qquad (21)$$

where g is the multi-scattering function defined by Eq. (4), γ is again the angle between $\overline{\mathrm{n}}$ and the line-of-sight. Let $\overline{*\oplus}$ be the unit vector along that direction. Eq. (21) becomes

$$\Delta F = \frac{F_\odot \, x}{2 \, g(Q, \alpha)} \left[(\overline{\mathrm{ki}} \wedge \overline{\mathrm{kj}}) . \overline{*\oplus} \right]^+ ; \qquad (22)$$

(the $^+$ means that only the positive values are kept; the negative ones are set to 0). Assuming that the polyhedron is convex, the total luminosity of the model is obtained by summing the ΔF corresponding to all the facets of the model. If the model is not convex, then there will be some shadowing effects and some of the facets will be partly hidden behind others. One could subtract the contribution of these effects to the total luminosity, but this would be too heavy from a computational point of view. Another possibility is to force the model to be convex. Formally, to be sure that a polyhedron is convex, one just has to check that the lines joining any pair of summits are completely inside the polyhedron. Again, this is to heavy to be checked in the kind of application we carried out. Therefore, we just force the

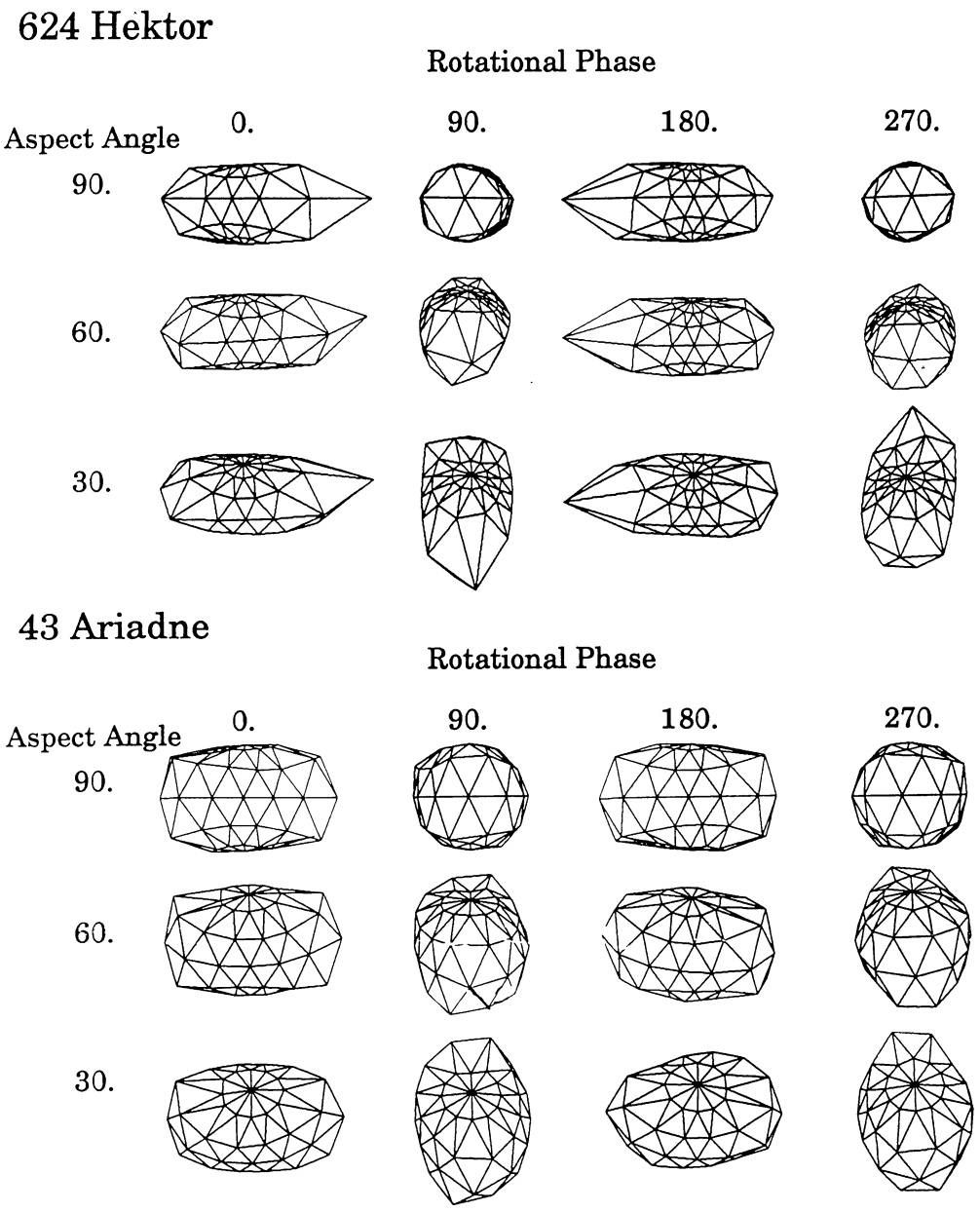

Fig. 4. Shape models obtained by the FS method for 624 Hektor and 43 Ariadne, seen at different aspect and rotational phase angles (in degree)

model to be "as convex as possible", and neglect the effects of the eventually remaining concavities. Two methods have been developed for that purpose.

The first one is based on the minimization of the surface to volume ratio of the asteroid model. This ensures that the model is as spherical as possible. A parameter allows us to tune this "spherisation". We usually select a low to intermediate spherisation, which is enough to make the concavity effects negligible. If the spherisation is too strong, the resulting model is nearly spherical. It does not reproduce the lightcurves anymore and is absolutely useless for the pole determination... All the polyhedrons were visually checked to verify that the convexity was reasonably satisfied. Figure 2.3 represents the models corresponding to the best pole orientation for 624 Hektor and 43 Ariadne.

The second method used to render the model as convex as possible is the maximization of the radii entropy (Schils 1991). Let us introduce the normalized radii:

$$p_i = \frac{r_i}{\sum_{\text{all}} r_i} \cdot \tag{23}$$

The entropy

$$S = \sum_{\text{all}} p_i \ln p_i \tag{24}$$

is maximal when all the p_i are equiprobable, that is when all the radii are equal. Again, we introduced a parameter allowing to tune the "spherisation" of the model.

To find the pole of the asteroid, the procedure is the same as for the FAM method: the sky is scanned, and for each trial pole orientation, Eq. (18) is minimized. The map of the resulting χ^2 is then plotted, and the pole identified. Two independent FORTRAN codes have been produced, corresponding to different modelings and to the two distinct spherisation methods. Both have been optimized to run mostly vectorially (90%) on our IBM. Both programs lead to very similar solutions.

Like the pseudo-albedo map of the FAM method, the shape model obtained by the FS method is only one among an infinity of solutions.

2.4. The Photometric Astrometry (PA)

The three previous methods use the relation between the photometry of the asteroid (magnitude or derived value) as a function of the geometry. The Photometric Astrometry, also called Epoch Method, interprets the correlation between the geometry and the slight variations of the observed rotational period.

The only assumption made in the PA is that a "lightcurve recognizable feature" (LRF) is present in all the observed lightcurves (Taylor 1979). This LRF has to be each time caused by the same geophysical or morphological feature (the RFO: recognizable feature origin), passing at the position corresponding to the best solar illumination, combined with the best diffusion towards the Earth. The LRF can be, for example, a maximum of the lightcurve and its RFO a bright spot. The LRF takes place when the RFO is closest to the middle of the arc between the sub-Earth and sub-solar points: this point defines the "phase angle bisector" (PAB, introduced by Magnusson 1986). This happens when the RFO and the PAB astrocentric longitudes are equal.

The epoch of the LRF is a function of the pole orientation. This is illustrated in Fig. 3, for the case of two example poles. Let M_a and M_b be the PABs corresponding to two distinct observations (independent of the pole orientation). The time laps between the two LRFs will be longer in one configuration than in the other, because the asteroid "has to rotate more" in order to bring the RFO from M_a to M_b. This accounts for the difference between the sidereal and synodic periods of rotation. This formalism is directly inspired from the one developed by P. Magnusson (1986).

Knowing the pole coordinates and the sidereal period in addition to the position of the asteroid, the Sun and the Earth for a selected epoch, it is possible to compute the epoch of any other LRF. In practice, only the synodic periods of rotation are given. The unknown pole orientation and sidereal period are found by minimizing the difference between the observed LRF t^{Obs} and the computed ones t^{Comp}, adjusting λ_o, β_o and T_{Sid} for the whole set of lightcurves available. The minimized quantity

Table 1. Aspect data; the distances are given in AU, λ, β and α in degrees

624 Hektor						
Date	λ	β	Δ	R	α	Ref.
1957 05 04	249.5	-22.1	4.212	5.088	6.2	DG69
1957 05 30	246.0	-22.6	4.142	5.093	4.4	DG69
1965 02 04	119.4	14.6	4.114	5.028	4.1	DG69
1967 03 07	192.9	-9.9	4.114	5.007	5.5	DG69
1968 05 01	225.8	-20.3	4.109	5.063	4.1	DG69
1984 10 03	7.9	10.1	4.310	5.300	1.8	*
1984 10 05	7.6	10.2	4.310	5.300	2.3	*
1991 04 14	212.3	-16.9	4.144	5.100	3.8	*
1991 04 18	211.9	-17.3	4.136	5.101	3.5	*
43 Ariadne						
Date	λ	β	Δ	R	α	Ref.
1965 05 01	221.8	-4.9	0.961	1.0079	2.5	VHG79
1965 05 03	221.3	-4.8	0.957	1.0084	2.6	VHG79
1972 08 09	344.6	6.3	0.982	1.0137	14.3	BM74
1972 08 13	343.9	6.4	0.972	1.0130	12.1	BM74
1982 10 15	13.8	5.8	1.200	0.9969	4.5	DMC84
1984 02 01	128.6	-4.1	1.524	0.9854	2.0	DM87
1984 02 20	123.8	-4.2	1.564	0.9986	10.3	W87
1985 08 16	319.8	6.2	0.891	1.0126	3.7	*

References: * = This work; DG69 = Dunlap & Gehrels 1969; VHG79 = Van Houten Groeneveld et al. 1979; BM74 = Burchi & Milano 1974; DMC84 = Di Martino & Cacciatori 1984; DM87 = Di Martino et al. 1987; W87 = Weidenschilling et al. 1987.

is

$$K^2(\lambda_o^{\mathrm{Trial}}, \beta_o^{\mathrm{Trial}}) = \sum_{\mathrm{Observations}} (t_i^{\mathrm{Obs}} - t_i^{\mathrm{Comp}})^2 \ . \qquad (25)$$

Like for the other methods, this is performed by scanning the (λ_o, β_o) space, minimizing K^2, and building a χ^2 (λ_o, β_o) map showing the best pole solution in its lowest valleys.

3. Pole determination of 624 Hektor and 43 Ariadne

We have applied the various pole determination methods described in Sect. 2 to the minor planets 624 Hektor and 43 Ariadne . The aspect parameters of the previously published and new lightcurves we used are listed in Table 1.

For both asteroids, the χ^2 maps corresponding to each method are given in Figs. 6 and 7. These global maps were generated scanning the λ_o, β_o space with a 10 degree step in both coordinates. The pole solutions were then found by local scans, performed with a 1^o step.

So, the pole solutions are defined with an internal precision of 1 degree. The real uncertainty on the poles is of course much larger. The best way to estimate it is to examine the valleys in the χ^2 maps. The shaded regions correspond to the pole orientation having a χ^2 lower than 1.1 time the minimum value of the valley. Even if it would be quite difficult to quantify it (i.e. in terms of σ), the confidence level to have the real pole inside that

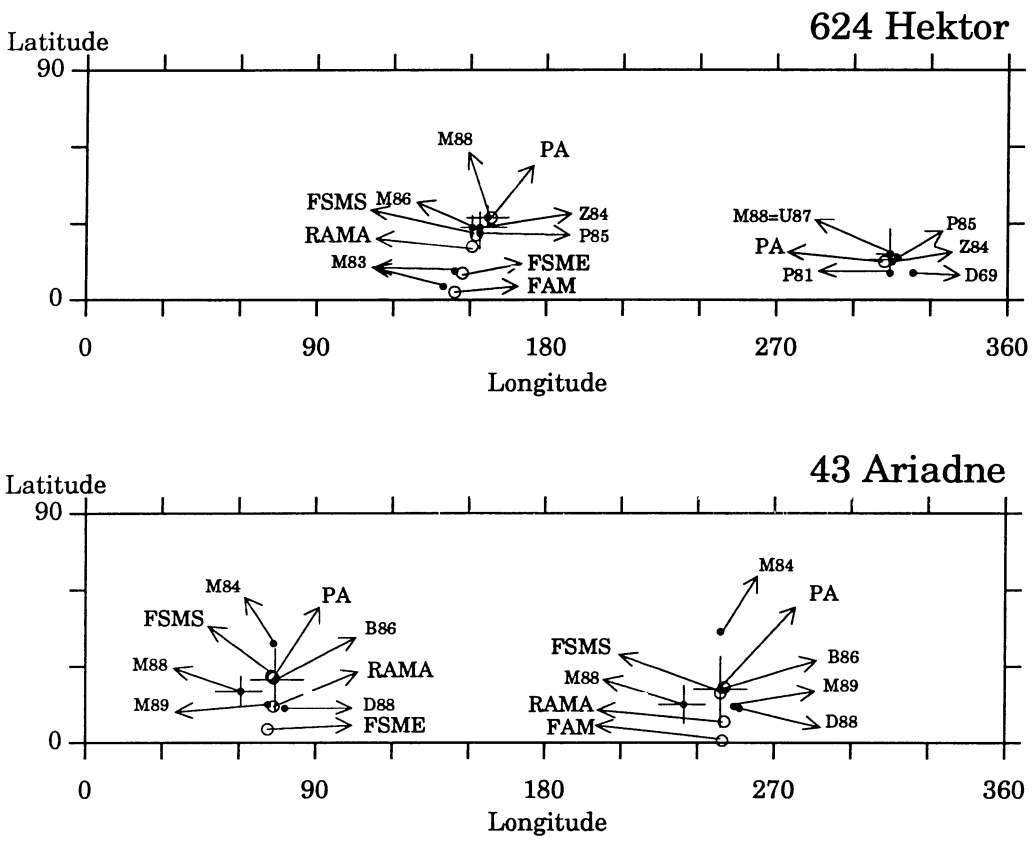

• Previous results (with error bars)

o Our results; for the uncertainty regions, refer to Figs. 9 and 10

Fig. 5. Comparison of the pole solutions obtained by us and other authors; when available, the error bar is plotted. For the error regions of our methods, refer to Figs. 9 and 10; Ref: 624 Hektor: D69 = Dunlap & Gehrels 1969, P81 = Poutanen et al. 1981, M83 = Magnusson 1983, Z84 = Zapallà & Knežević 1984, P85 = Pospieszalska-Surdej & Surdej 1985, M86 = Magnusson 1986, U87 = Uchida & Goguen 1987, M87 = Michaloski 1988; 43 Ariadne: M84 = McCheyne et al. 1984, B86 = Barucci et al. 1986, M88 = Michalowski 1988, D88 = Drummond et al. 1988, M89 = Magnusson 1989; FSMS refer to the FS method with minimization of the Surface/Volume ratio, while FSME to the FS method with maximization of entropy

region if very high. We will use it as the uncertainty region. As these regions are elongated in a direction which is not parallel to the coordinate axes, it is not very interesting to give errors on the λ_o, β_o. We have listed in Table 2 the coordinates of the best and secondary pole solutions, as well as all the other parameters relevant for the different methods. The best and secondary solutions correspond to the absolute and first relative minima in the maps, respectively. In Fig. 4, we have plotted the shape model corresponding to the best pole solution, using the surface/volume minimization. The maximization of entropy, with a similar number of facets, leads to an equivalent shape model.

In Fig. 5, we have plotted for both 624 Hektor and 43 Ariadne the pole solutions, as obtained by our four methods and by other authors.

4. Discussion

As shown in the previous section, there is a very good agreement between the methods described in this paper, and between our results and those already published by other authors. The precision of an early version of our FAM method (Hainaut et al. 1990) has been tested during the A.C.M. III meeting (held in Uppsala, June 1989). H. Karttunen provided us with a set of synthetic lightcurves and the corresponding ephemeris data (but no information on the pole orientation, the shape nor the albedo). The best pole solution we found lied at less than 6 degree of the real pole (Karttunen et al. 1989).

There is a common point between all the pole determination methods we have described: the lowest valleys in the χ^2 maps are very elongated in one direction and very narrow in the perpendicular direction. For the photometric methods (RAMA, FAM and FS), they are roughly elongated in the β_o direction,

Table 2. Pole solutions for the different methods; λ_0 and β_o are the ecliptic coordinates of the pole; a, b, c are the ellipsoid semi-axes; Q is the multiple scattering parameter; T is the sidereal period

Method	Solution	Pole	Additional parameters
624	**Hektor**		
RAMA	Best Solution	$\lambda_0 = 315^o$ $\beta_0 = -16^o$	a/b = 2.27 ; b/c = 1.41
	Secondary Solution:	$\lambda_0 = 152^o$ $\beta_0 = +27^o$	a/b = 2.26 ; b/c = 1.32
FAM	Best Solution (72 facets)	$\lambda_0 = 145^o$ $\beta_0 = +3^o$	$Q = 0.717$
FAS	**Minimization of S/V** (80 facets)		
	Best Solution	$\lambda_0 = 149^o$ $\beta_0 = +22^o$	$Q = 0.38$
	Maximisation of Entropy (80 facets)		
	Best Solution	$\lambda_0 = 144^o$ $\beta_0 = +11^o$	$Q = 0.35$
PA	Best Solution	$\lambda_0 = 156^o$ $\beta_0 = +33^o$	$T = 6.9205094$ h $\pm 1.0 \times 10^{-6}$ (Retrograde)
	Secondary Solution	$\lambda_0 = 313^o$ $\beta_0 = +17^o$	$T = 6.9205109$ h $\pm 1.3 \times 10^{-6}$ (Retrograde)
43	**Ariadne**		
RAMA	Best Solution	$\lambda_0 = 72^o$ $\beta_0 = +13^o$	a/b = 1.84 ; b/c = 1.53
	Secondary Solution	$\lambda_0 = 250^o$ $\beta_0 = +8^o$	a/b = 1.84 ; b/c = 1.50
FAM	Best Solution (72 facets)	$\lambda_0 = 250^o$ $\beta_0 = +1^o$	$Q = 0.192$
FAS	**Minimization of S/V** (80 facets)		
	Best Solution	$\lambda_0 = 248^o$ $\beta_0 = +20^o$	$Q = 0.098$
	Secondary Solution	$\lambda_0 = 73^o$ $\beta_0 = +25^o$	$Q = 0.092$
	Maximisation of Entropy (60 facets)		
	Best Solution	$\lambda_0 = 70^o$ $\beta_0 = +5^o$	$Q = 0.19$
PA	Best Solution	$\lambda_0 = 250^o$ $\beta_0 = +22^o$	$T = 5.7619820$ h $\pm 0.6 \times 10^{-6}$ (Retrograde)
	Secondary Solution	$\lambda_0 = 74^o$ $\beta_0 = +24^o$	$T = 5.7619819$ h $\pm 0.9 \times 10^{-6}$ (Retrograde)

while the PA's valleys are nearly perpendicular. This perpendicularity was very generally obtained for all the asteroids that were studied by our group, including synthetic data (Detal et al. 1992) and other real asteroids (unpublished results), and also by Magnusson (1986, 1992). The accuracy of the photometric methods is very good in longitude, and the chronometric one is very good in latitude. It corresponds to the fact that they use completely independent and complementary information from the lightcurves. As a consequence, a pole determination should always include both kinds of technique, and their results should be combined. An improvement could be to build a new lightcurve analysis method featuring a complete and simultaneous modeling of the lightcurve in epoch and magnitude.

For low orbital inclinations, all the methods lead to two main χ^2 valleys, corresponding to the real pole (λ_o, β_o) and its mirror ($\lambda_o + 180^o$, β_o). It was shown by Russell (1906) that for $i = 0^o$, the photometric lightcurves allow to find the value of the inclination of the rotation axis, but not its sign. For larger i, this effect is less sensible. It would of course be interesting to eliminate this indetermination. This could be done by observing the considered asteroid when the predicted amplitude difference between the two possible poles is as large as possible. For 624 Hektor and 43 Ariadne , we have computed what will be the difference $\Delta m_{P1} - \Delta m_{P2}$between the predicted lightcurve amplitudes for both possible poles, using the RAMA poles coordinates and ephemerides for next years. Figures 8 and 9 show this difference in amplitude as a function of the asteroid longitude.

The albedo distributions and shapes derived by the FAM and FS methods are only internal models used to determine the pole. Even if they constitute a possible representation of the real characteristics of the minor planet, they are only one among an infinity of equivalent solutions. The maximization of entropy or minimization of S/V ratio used in the FS method ensure that the resulting model is more realistic than others, but this is not sufficient. Moreover, the real asteroid will more likely have a complex shape and albedo distribution, not only one or the other as in the present models. It is however important to note that this does not affect at all the quality of the pole solutions: even if the derived model is very different from the real asteroid, its lightcurves match at best the observed ones. A very realistic model (within the limitations of the method) would be equiva-

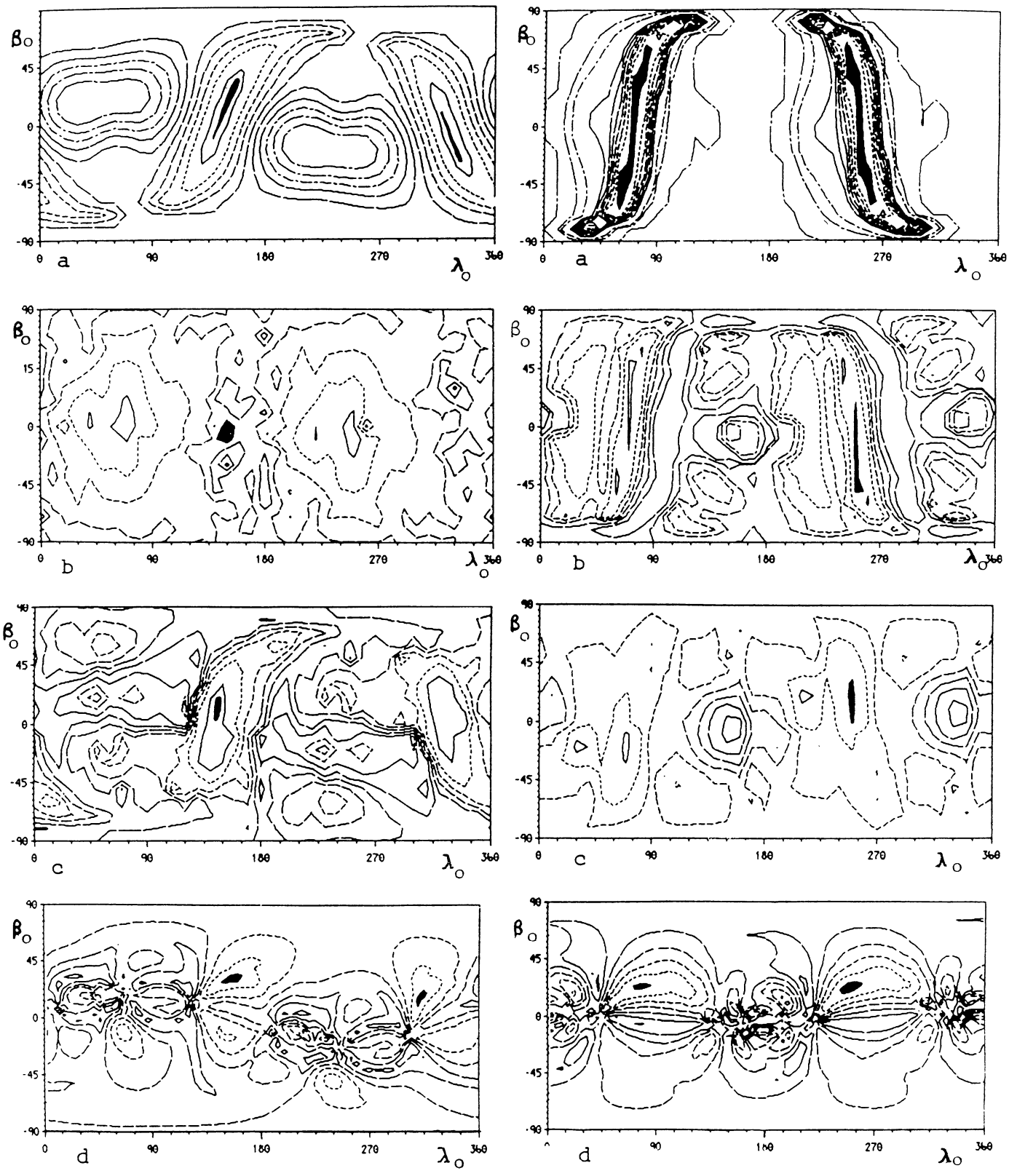

Fig. 6. a–d. The χ^2 maps obtained for 624 Hektor by the RAMA method **a**, the FAM method **b**, the FS method **c** and the PA **d**; the lowest regions are shaded

Fig. 7. a–d. The χ^2 maps obtained for 43 Ariadne by the RAMA method **a**, the FAM method **b**, the FS method **c** and the PA **d**; the lowest regions are shaded

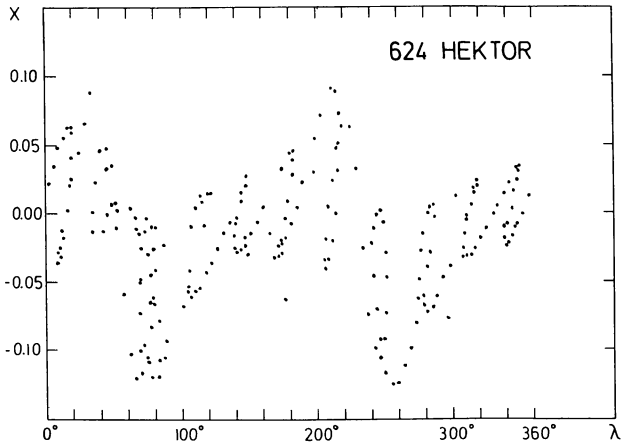

Fig. 8. Difference between the predicted lightcurve amplitudes for the two possible pole solutions derived for 624 Hektor by the RAMA method

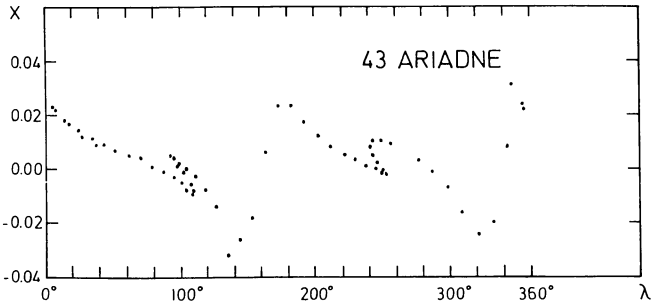

Fig. 9. Difference between the predicted lightcurve amplitudes for the two possible pole solutions derived for 43 Ariadne by the RAMA method

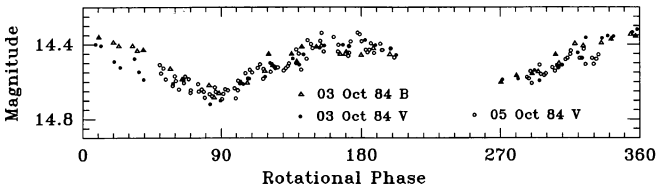

Fig. 10. 624 Hektor: Composite V lightcurve, with the V and B data obtained on October 3, 1984, and the V data on October 5

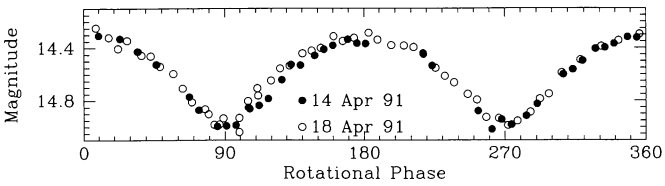

Fig. 11. 624 Hektor: V lightcurve obtained on April 14 and 18, 1991

lent to the computed one from the χ^2 point of view. The only way to obtain this realistic shape and albedo model of a minor planet from photometric observations is to mix lightcurves in the visible band with others obtained simultaneously in the thermal infrared. The information contained in these data is complementary: an observed flux increase can be caused either by a cross-section increase or by a bright spot apparition. The IR lightcurves should enable one to discriminate between these possibilities, as the cross section variation will be the same as in the visible, while the low thermal emissivity of a bright spot will cause a diminution of the IR flux. A new Free Albedo and Shape method giving the complete albedo and shape model is being presently tested on some experimental observations that we have obtained at la Silla.

Acknowledgements. We are very grateful to P. Collette, who conceived and realized many nice and efficient graphical softwares allowing us to visualize our models and their lightcurves.

Appendix A: observations

The positions and aspect data have been computed using the programs POS and EPH, designed and kindly put at our disposal by R.M. West (E.S.O.).

The photometric data are available in a digital form (PC floppy or electronic mail) upon request to A.D.

A.1. 624 Hektor

A.1.1. The 1984 opposition

Four nights of observations (October 2-5, 1984) with the ESO 1m telescope had originally been allocated to our photometric study of 624 Hektor at La Silla (Chile). Because of bad meteorological conditions, two nights were completely lost. Standard UBV photometry was carried out on October 3. However, this night was not of very good photometric quality, due to a high content of humidity in the air and a strong wind. As a result, the U measurements of both the asteroid and the comparison star showed an abnormally large scatter. As the strong wind persisted on October 5, we decided to perform measurements only in the V filter.

The observations were performed with a single channel photometer equipped with an EMI 6256 photomultiplier, standard filters for the UBV magnitudes, a dry-ice cooling system and the standard ESO pulse counting electronics. A basic integration time varying between 30 and 60 seconds was chosen while collecting the photons through a 22 arcsecond diaphragm. The general observing routine included frequent measurements of the asteroid, sky, comparison star and some E-Region standard stars (Cousins & Stoy 1962).

The data were reduced to the standard UBV system in the usual way, taking into account the first and second order extinction as well as linear color transformations using the ESO Snopy photometric package. The V measurements recorded on October 5, 1984 have also been transformed to the standard UBV

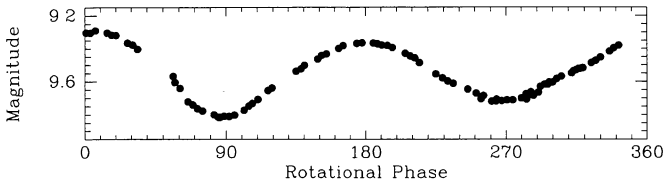

Fig. 12. 43 Ariadne: V lightcurve obtained on August 16, 1985

Table 3. Positions of the asteroids and comparison stars

Object	Date UT	RA_{1950} h m s	Dec_{1950} ° ' "	V
624 Hektor	1984 10 03	00 11 01	+12 07 52	Fig. 10
	1984 10 05	00 12 33	+12 25 37	Fig. 10
Comp. Star	-	00 11 28	+12 21 54	12.80
624 Hektor	1991 04 14	13 34 37	-28 18 33	Fig. 11
	1991 04 18	13 32 12	-28 13 25	Fig. 11
SAO 181869 Comp. Star	-	13 38 55	-29 00 17	9.99
43 Ariadne	1985 08 16	21 21 00	-08 58 21	Fig. 12
BD-9°5738 Comp. Star	-	21 17 00	-09 16 42	9.46

system. Since the B-V color index (0.703) obtained during the first night did not show any variation exceeding the mean scatter (± 0.050 mag.) of the observations, we have illustrated in Fig. 10 the V photoelectric data recorded on October 3 and 5 as well as the B measurements, offset by -0.703 mag. In this figure, the magnitudes of the composite lightcurve have been plotted as a function of the rotational phase. The phase origin corresponds to the flux maximum that took place at 3 h 14 min 46 sec UT on October 3, and the synodic period of rotation was 6.9286 h. The ordinates refer to the V magnitude observed on October 3, 1984, with no correction for the distance and the solar phase effects.

A.1.2. The 1991 opposition

In April 1991, 13 nights were attributed to our observing program on the ESO 50cm telescope, at la Silla. Hektor was observed during the nights of April 13-14 and 17-18, 1991, in good photometric conditions. The observations were performed with a single channel photometer, equipped with a Hamamatsu photomultiplier (Pelletier cooling), and the standard filters for UBVRI photometry. Hektor was measured only in the UBV filters, through a 21 arcsecond diaphragm. The integration time was optimized in the 20 to 80 second range. The observation and reduction procedures were similar to those used in 1984.

The resulting V lightcurve is plotted in Fig. 11 (without distance nor solar phase corrections), and the aspect and photometric data parameters are listed in Tables 1 and 3. The rotational phase origin corresponds to the maxima that took place at 5 h 40 min 6 sec UT on April 14, 1991, and at 6 h 34 min 30 sec UT on April 18. The synodic period of rotation was 6.9226 h.

The asteroid did not show any significant color variations during these observations.

A.2. 43 Ariadne

This asteroid has been observed photometrically on August 16, 1985, with the ESO 50cm telescope. The observing and reduction procedures were very much the same as those described for 624 Hektor in 1984. A 19 arcsecond diaphragm was selected, and the integration time varied between 20 and 40 seconds. Figure 12 displays the V photometric measurements without distance nor solar phase corrections. The rotational phase origin corresponds to the maximum that occurred at 3 h 18 min 03 sec UT on August 16, 1985. The synodic period of rotation was 5.800 h. Aspect and photometric data referring to these observations are also summarized in Tables 1 and 3.

References

Barucci, M. A., Bockelée-Morvan, D., Brahic, A. et al. 1986, A&A 163, 261
Burchi, R., Milano, A., 1974, A&AS 15, 173
Cousin, A. W. J., Stoy, R. H., 1962, Royal Obs. Bull, 49
Detal, A., 1988, Master Thesis, University of Liège
Detal, A., Schils, P., Collette, P. et al. 1992, in the proceedings of the 30th Liege International Astrophysical Colloquium "Observations and physical properties of small solar system bodies", eds. A. Brahic, J.-C. Gerard and J. Surdej, p. 181
Di Martino, M., Cacciatori, S., 1984, Icarus 60, 75
Di Martino, M., Zapallà, V., de Sanctis, G., Cacciatori, S., 1987, Icarus 69, 338
Drummond, J. D., Weidenschilling, S. J., Chapman, C. R., Davis, D. R., 1988, Icarus 76, 19
Dunlap, J. L., Gehrels, T., 1969, AJ 74, 796
Hainaut, O., Detal, A., Ibrahim-Denis, A., Surdej, J., 1989, in: Asteroids, Comets, Meteors III, eds. C.-I. Largerkvist, H. Rickman, B.A. Lindblad and M. Lindgren, p 99
Hainaut, O., Detal, A., 1992 in preparation
Karttunen, H., Cellino, A., Detal, A. et al. 1989, in: Asteroids, Comets, Meteors III, eds. C.-I. Largerkvist, H. Rickman, B.A. Lindblad and M. Lindgren, p 119
Lagerkvist, C.-I., Barucci, M. A., Capria, M. T. et al. 1987, in: Asteroid Photometric Catalogue, ed. Consiglio Nazionale delle Ricerche, Roma
Lagerkvist, C.-I., Barucci, M. A., Capria, M. T. et al. 1988, in: Asteroid Photometric Catalogue — First update, ed. Consiglio Nazionale delle Ricerche, Roma
Lumme, K., Bowell, E, 1981 a, AJ, 86, 1694
Lumme, K., Bowell, E, 1981 b, AJ, 86, 1705
Magnusson, P., 1983, in Asteroids, Comets, Meteors, eds. C.-I. Lagerkvist and H. Rickman, Uppsala Univ., Uppsala, p. 77
Magnusson, P., 1986, Icarus 68, 1
Magnusson, P., 1989, in: Asteroids II, eds. R.P. Binzel, T. Gehrels and M. Shapley Matthews, The University of Arizona Press, Tucson, p. 1180

Magnusson, P., 1992, in the proceedings of the 30th Liege International Astrophysical Colloquium "Observations and physical properties of small solar system bodies", eds. A. Brahic, J.-C. Gerard and J. Surdej, p. 163
McCheyne, R. S., Eaton, N., Green, S. F., Meadows, A.J., 1984, Icarus 59, 286
Michalowski, T., 1988, Acta Astron. 38, 455
Pospieszalska-Surdej, A., Surdej, J., 1985, A&A, 149, 186
Poutanen, M., Bowell, E., Lumme, K., 1981, BAAS 13, 725
Russell, H.N., 1906, ApJ 24, 1
Schils, P., 1991, Master Thesis, University of Liège
Surdej, J, Pospieszalska-Surdej, A., Michalowski, T., Schober, H.J., 1986, A&A 170, 167
Taylor, R., 1979, in: Asteroids, ed. T. Gehrels, The University of Arizona Press, Tucson
Taylor, R, Birch, P.V., Drummond, J. et al. 1987, Icarus, 69, 354
Uchida, K., Goguen, J. D., 1987, BAAS 19, 842
Van Houten-Groeneveld, I., Van Houten, C.J., Zappalla, V., 1979, A&AS 35, 223
Weidenschilling, S.J., Chapman, C.R., Davis, D.R. et al. 1987, Icarus 70, 191
Zappalà, V., Knežević, Z., 1984, Icarus 59, 436

This article was processed by the author using Springer-Verlag LaTeX A&A style file version 3.